Attenuation of direct solar radiation by a perforated plate for on-orbit visible calibration

James C. Bremer[a], H. John Wood[b], Guojun Si[a]
[a]Swales Aerospace, 5050 Powder Mill Rd., Beltsville, MD, 20705
[b]Goddard Space Flight Center, Greenbelt, MD, 20771

ABSTRACT

Attenuated sunlight is a valuable reference for on-board calibration of spaceborne instruments that observe reflected sunlight from the earth. Direct viewing of the sun through a perforated plate can provide full aperture, end-to-end calibration. Since the transmissivity of the perforated plate depends only upon its geometry, it is potentially more stable than the diffuse reflectivity of a diffuser plate, particularly when exposed to the space environment. We have observed the sun through a sheet metal plate with a hexagonal array of small holes placed in front of a telescope. A pinhole in the telescope's focal plane, followed by a spectral filter and a silicon photo-diode, were selected to approximate the IFOV and spectral bands proposed for imagers on future GOES missions. In each observation, the center of the solar image was found to have a smooth, symmetrical maximum, with no significant angular structure due to interference. These observations demonstrated that the perforated plate technique is a promising method for stable, long-term, on-orbit calibration of visible and near IR channels on spaceborne optical instruments.

Keywords: calibration, remote sensing, albedo, visible, GOES

1. CALIBRATION SOURCE REQUIREMENTS

Imagers on the next generation of the Geostationary Operational Environmental Satellite (GOES) system have a goal to calibrate all sunlit channels with errors below 5% for absolute radiance level (accuracy) and below 1% for relative error (precision) over a mission lifetime of seven years[1,2]. Many remote sensing instruments that are planned for operation in low-earth orbit (LEO) will have similar goals or requirements. To achieve the necessary precision, any calibration technique must illuminate the instrument with a level of input radiance that remains stable within a few tenths of 1%. Reliable calibration also requires that the radiation from the calibration source follow the same path through the instrument as radiation from the scene. If the system has a movable optical element with a variable incidence angle, such as a scan mirror, then calibration measurements at several incidence angles are desirable.

The calibration source should provide uniform illumination over the full aperture. It is also preferable to use an unpolarized source with a broad spectrum of radiation at a color temperature approximately equal to that of the sun. Since earth-viewing imagers observe spatially extended targets, their calibration source should be uniform over a solid angle that is large in comparison to the instantaneous field of view (IFOV) of their detector elements. To accommodate future missions, the technique should be capable of operating throughout the spectral range of reflected sunlight from the earth, including the visible, near infrared (NIR), short-wave infrared (SWIR), and near ultraviolet (NUV).

The gain of a channel can best be determined by taking two measurements: one with no external input radiance, to measure the offset due to dark current, and a second with a known input radiance. Spaceborne sensors can measure the offset by viewing deep space, pointing at an angle that avoids the earth, sun, moon, and any planets or stars that are bright enough to corrupt the measurement. Thermal radiation from within the instrument is negligible at these short wavelengths, so the aperture can also be blocked to perform this offset measurement.

For the greatest accuracy, the second measurement should be made near the top of the channel's dynamic range. (If the gain is not linear, measurements at intermediate radiance levels may also be required.) At visible wavelengths, clouds and snow often approximate an ideal Lambertian surface that reflects diffusely. Consequently, the sunlit channels on many earth-viewing remote sensing instruments are designed so that the high end of their dynamic range corresponds to a radiance level approximately equal to a 100% albedo.

The calibration source must be observable frequently enough to track long-term changes in these channels. Techniques requiring a celestial body within the field of regard (FOR) of the instrument may be constrained to

infrequent time intervals when this condition is satisfied. If this source is not observable frequently enough, or at all, in normal operations, then it may be necessary to interrupt routine data-taking and rotate the entire spacecraft to view the source. It is also desirable to minimize the amount of time required for calibration, the complexity of mechanisms, the momentum disturbance that they create, and the power, volume, mass, and cost of the calibration hardware. Any calibration technique that blocks the line of sight of the instrument could result in loss of the mission if it became jammed in this position. Therefore, it is prudent to equip such a calibration system with redundant retraction mechanism.

2. CONVENTIONAL SOLAR CALIBRATION TECHNIQUES

The present GOES Imager has no onboard calibration apparatus for its visible channel, but long-term trends in its throughput have been tracked by observing a variety of vicarious calibration sources. These sources include the moon[3], stars[4], and selected, radiometrically stable desert areas on the earth's surface in conjunction with simultaneous observations from aircraft along a contiguous atmospheric path.[5] On future missions, these vicarious calibration techniques may be augmented with an onboard calibration system that attenuates direct sunlight. A sub-aperture technique, in which the sun is viewed directly through a single small aperture, can provide some indication of throughput changes. However, it cannot accurately account for vignetting due to alignment shifts or for degradations such as contamination and coating de-lamination that may not be uniformly distributed across an optical surface.

Some instruments that are currently flying on the EOS-AM (Terra) spacecraft at LEO are calibrated by observing a diffuser plate, inserted in front of the aperture of the system and illuminated by direct sunlight. The surface of this plate is coated with a diffusely reflective material that approximates an ideal Lambertian radiator. This technique has also been proposed for future geosynchronous imagers. The diffuser plate calibration technique has a number of beneficial features. It can be performed by inserting the diffuser plate in front of the aperture of the optical system in a position where the plate is illuminated by direct sunlight, so it does not require that the sun lie within the field of view (FOV) of the instrument. If the diffuse surface is an ideal Lambertian radiator and it overfills the aperture of an optical instrument, then the radiance observed by that instrument is independent of the angle of observation. If the sunlight illuminates the diffuser plate along its normal axis, then the radiance is also insensitive to first-order tilt of the plate. The diffuser plate illuminates the entire FOV of the instrument.

The major problem with the diffuser plate is the progressive degradation of its diffusely reflective surface in the space environment. There are multiple mechanisms that cause this degradation, including contamination, vacuum UV (VUV) radiation, micro-meteoroids, and atomic oxygen. Contaminants that luminesce when exposed to UV radiation are another potential problem. To mitigate these problems, an independent monitoring sensor, designed for high stability, may also have to be flown onboard the spacecraft.

Since the diffuse surface is not an ideal Lambertian reflector, it must be measured extensively to characterize and compensate for its bi-directional reflectance distribution function (BRDF) as a function of wavelength and polarization. It is also necessary to minimize sun glints on the deployed the diffuser plate. This constraint is particularly important for imagers in geosynchronous orbit, where reflective baffles and thermal control surfaces are often used to minimize the effects of solar intrusion.

3. PERFORATED PLATE CALIBRATION TECHNIQUE

As an alternative to the diffuser plate, we have proposed viewing the sun directly through an attenuator fabricated by drilling a large array of holes with diameters in the 50-100 μm range into an opaque plate. This plate is deployed in front of the aperture of the optical system for solar calibration and is stowed during earth observations. The perforated plate attenuates the radiance at the center of the solar disk to a level that lies within the dynamic range of each channel. There are two factors that contribute to this attenuation: the overwhelming majority of the radiation is blocked and the small fraction that is transmitted is diffracted into a blurred image whose diameter exceeds that of the solar disk. Diffraction will also smear out structure in the solar image, due to sunspots, flares, and limb darkening. Each detector element is calibrated by scanning its line-of-sight (LOS) through the center of the diffracted solar image. Like the diffuser plate technique, this perforated plate technique is capable of providing a well-characterized, uniform radiance source at a high albedo level for full-aperture, end-to-end calibration. When the perforated plate is normal to the sun line, the diffracted radiation is unpolarized and insensitive to tilt.

The perforated plate's throughput depends only upon its geometry, giving it greater long-term stability than the

reflectivity of a diffuser plate. The perforated plate must be shielded from contaminants when not in use, but it is far less sensitive to contamination than a diffuser plate. For comparison, a hydrocarbon contaminant layer only a few nanometers thick, deposited of the surface of a diffuser plate and polymerized by vacuum ultraviolet (VUV) radiation in space, can produce a significant decrease in its reflectivity, particularly at ultraviolet and short visible wavelengths.[6,7,8] This same level of contamination would have a negligible effect on the throughput of holes 50-100 μm in diameter.

Since the perforated plate calibration technique requires that the sun lie within the FOR of the instrument, its availability may be more restricted than that of a diffuser plate technique. A nadir-viewing satellite in LEO requires an attitude maneuver to view the sun. Since attitude maneuvers are very undesirable for an operational GOES satellite, the perforated plate calibration can only be performed when the sun passes through the FOR of the instruments, near local midnight during seasonal periods of slightly less than two months centered around each equinox. It also requires virtually light-tight insertion of the perforated plate into the optical path, ideally with less than 10^{-7} leakage.

The perforated plate calibration can best be implemented by scanning the detectors through the central maximum of the diffracted solar image where the radiance is at least 99% of its peak value. For hole diameter in the 50-100 μm range, we have found that this maximum has a diameter of less than one milliradian. Thus, calibration of an instrument whose FOV exceeds the width of this maximum requires multiple scans through the diffracted solar image.

Solar limb darkening decreases the effective width of the solar disk, and becomes more pronounced at shorter wavelengths. The image broadening produced by diffraction also decreases rapidly with decreasing wavelength. In combination, these two effects causes the width of the diffracted solar image to decrease rapidly and the effective albedo at the peak to increase sharply with decreasing wavelength. This strong wavelength dependence implies that a single perforated plate cannot provide a high albedo reference at the maximum of the solar image over a wide spectral range. On the other hand, if the measured shapes of the diffracted solar images remain constant in all channels throughout a mission, it provides an independent verification that the hole diameter in the perforated plate has also remained constant and that the spectral passbands of the channels have not shifted.

One major concern in using a regular array of holes as an attenuator is that it might produce an interference pattern with enough angular structure to make the calibration data difficult to interpret. When illuminated by collimated, monochromatic light, a regular, hexagonal array of holes produces a hexagonal diffraction pattern that is the two-dimensional Fourier transform of the array. If the separation distance between adjacent holes is S, then separation between adjacent rows in the perforated plate is 0.866S. The angular separation between adjacent interference maxima is $8/(0.866S) = 1.1158/S$. For a wavelength of $\lambda = 750$ nm and a separation between holes of S = 5 mm, this anglar separation between adjacent interference maxima becomes 0.17 mrad, which is much smaller than the 9.3 mrad diameter of the sun's photosphere. The diffraction pattern is suppressed because the angular extent of the source is much greater than this angular separation between these interference maxima. The finite spectral bandwidths of the channels also help to suppress the interference pattern by dispersing all maxima except the zero order. Thus, the light that impinges on a given photodetector in the instrument's focal plane originates predominately from those areas on the solar disk where there is a positive interference pattern created by the regular hexagonal array. However, there are so many diffraction orders within the angular diameter of the solar disk and enough overlap among the higher orders that the radiance distribution is relatively free of angular structure.

4. PERFORATED PLATE APPARATUS

Our experiments were undertaken as part of a study of the Advanced Geosynchronous Studes Imager (AGSI) activity performed by NASA/GSFC. We assembled an experimental apparatus to verify the viability of the perforated plate technique. The primary objective of our experiment was to confirm our theoretical prediction that the diffracted solar image would have a maximum suitable for calibration, with minimal angular structure due to interference. Other objectives where to characterize the width of the diffracted solar image in each spectral band and to estimate the effective albedo level at the center of the solar image in each spectral band.

These experiments were performed with a telescope that had a clear aperture diameter of 178 mm and a focal length of 2413 mm. A pinhole 30 μm in diameter was placed in the telescope's focal plane, where it subtended 12.4 μradians in object space. This IFOV is comparable to the 14 μradian IFOV planned for future imagers in geostationary orbit, where it corresponds to a 0.5 km footprint at nadir. Each of three filters, in sequence, was

placed behind the pinhole and in front of a silicon photodiode. The spectral bandwidths of the three filters were all in the range from 90 nm to 100 nm, and their central wavelengths were approximately 450, 550, and 750 nm. These filters were chosen from "off-the-shelf" hardware as reasonable approximations of the passbands of the two visible channels and one near IR (NIR) channel proposed for the AGSI.

The perforated plate filter telescope was made from a sheet metal disk to avoid electrostatic problems. The diameter of the disk was slightly larger than the aperture of the telescope. The holes, drilled with an excimer laser, were tapered, and their cross-sections were not always circular. The plate was mounted inside a cylindrical baffle, perpendicular to the axis of the cylinder with the smaller cross-section of the tapered holes facing outward. The interior end of the barrel of this assembly was fitted with a screw thread that allowed it to be attached as an extension to the existing telescope tube.

The radiance that corresponds to a 100% albedo is the irradiance of the sun divided by π steradians. In determining specifications for the plate, we neglected the effect of solar limb darkening, and assumed that the solar irradiance would be uniform over the disk of the photosphere. Since the sun subtends a disk with a diameter of 0.0093 steradian and a solid angle of about 68×10^{-6} steradian, the throughput, T, of the perforated plate was specified to be about $68 \times 10^{-6}/\pi$ or 21.6×10^{-6}.

This approximation overestimated the throughput necessary to approximate a 100% albedo level when viewing the center of the solar disk. A more realistic estimate of the required throughput can be obtained by dividing the solid angle subtended by the disk whose diameter is full-width/half-maximum (FWHM) of the solar image at each wavelength by π steradians. The FWHM of the solar disk decreases with decreasing wavelength.[9] Table 1 gives the values of the FWHM(λ) in radians, $\Omega(\lambda)$, the effective solid angle of the solar disk in steradians, and $T_{req}(\lambda)$, the estimated value of the throughput required to obtain an effective albedo of 1.0, for each of the spectral bands.

Table 1. Estimated throughput levels required to obtain an effective albedo of 1.0

λ	FWHM(λ)	$\Omega(\lambda)$	$T_{req}(\lambda)$
450 nm	0.0072	40.7×10^{-6}	13.0×10^{-6}
550 nm	0.0078	47.8×10^{-6}	15.2×10^{-6}
750 nm	0.0087	59.4×10^{-6}	18.9×10^{-6}

The estimated throughput of the perforated plate, $T_{est}(\lambda)$, is the product of two factors: T_b, due to blockage, and $T_d(\lambda)$, due to diffraction. T_b is simply the ratio of the area of the holes to the total area. For circular holes of diameter D, oriented on a regular hexagonal array with a spacing of S between adjacent holes, T_b becomes:

$$T_b = (\pi D^2/4)/(0.866 S^2) = 0.907(D/S)^2 \quad (1)$$

$T_d(\lambda)$ is the wavelength-dependent reduction in radiance at the center of the diffracted solar image. It was estimated by convolution of the solar image with the Airy disk produced by a single hole. Based on this analysis, the perforated plate was specified to have holes of diameter, D =50 μm arrayed in a hexagonal pattern with a spacing of S = 5.0 mm between adjacent holes, producing a value of T_b equal to 90.7×10^{-6}. At a wavelength of λ = 650 nm , the value of T_d (8) was estimated to be 0.212. The product of these two attenuation factors yielded a total throughput of $T = 19.2 \times 10^{-6}$. This value is characteristic of a high albedo target when limb-darkening is neglected[10]:

When we measured the perforated plate, the average spacing between holes in the hexagonal array was S = 4.95 mm. The measured diameters of the holes in the perforated plate were considerably larger than their specified value of 50 μm, however. We measured the diameters of 25 holes, selected at random, and found that they varied from D = 59 μm to D = 109 μm.The average area corresponded to a hole diameter of D = 86.4 μ.m, from which the experimental value of $T_b = 276 \times 10^{-6}$. Table 2 lists the theoretical values of $T_d(\lambda)$ for a hole diameter of D = 86.4 μm, $T_{est}(\lambda)$, the estimated throughput equal to the product of T_b and $T_d(\lambda)$, and $ALB_{th}(\lambda)$, the theoretical estimate of the effective albedo of the perforated plate at each wavelength. The values of $ALB_{th}(\lambda)$ are derived by dividing the estimated throughput, $T_{est}(\lambda)$, by the required throughput, $T_{req}(\lambda)$, as listed in the right column of Table 1.

Table 2. Theoretical estimates of the effective albedo of the perforated plate

λ	$T_d(\lambda)$	$T_{est}(\lambda)$	$ALB_{th}(\lambda)$
450 nm	0.50	138×10^{-6}	10.6
550 nm	0.45	124×10^{-6}	8.2

750 nm	0.33	91×10^{-6}	4.8

By neglecting solar limb darkening, we overestimated the required transmissivity when determining the specifications for the perforated plate. The oversized holes produced larger than specified values of both T_b and $T_d(\lambda)$. When all of these factors are considered, the center of the diffracted solar disk viewed through the perforated plate is predicted to produce a radiance approximately one order of magnitude larger than a full albedo in the visible spectral range. This radiance, of course, increases rapidly with decreasing wavelength.

It is important to recognize that the above estimation of the effective albedo of the plate is based upon limited measurements and crude approximations. A more precise prediction would require more rigorous measurements of the distribution of the size and shape of the holes. It would then be necessary to calculate the convolution of the blur circle due to diffraction with the radial distribution of solar radiance as a function of angle, integrated over each spectral band.

5. PERFORATED PLATE EXPERIMENT PROCEDURE

All of our measurements were preformed around local noon (noon EST or 1 PM DST) on days when the atmosphere was exceptionally clear (for the Washington, D.C. area). On any given day, the atmospheric attenuation of sunlight remained virtually constant over the time interval of the experiment.

Preliminary experiments were performed at the Goddard Astronomy Club's facility at GSFC's Optical Test Site (OTS) on July 11, 1997 and September 5, 1997. The telescope, without the perforated plate filter assembly, was focused on a distant object, forming a sharp image on the pinhole. The perforated plate assembly was then attached. Its aperture was covered, and the electronic signal from the detector was nulled to subtract the dark current. The telescope was pointed slightly less than one degree to the west of the center of the sun. The pointing angle was held stationary and the sun was allowed to drift through its FOV. The signal from the silicon detector was sampled at 3-second intervals and correlated with the solar precession rate to determine the radiance as a function of angle. The spectral filter between the pinhole and the detector was changed and this procedure was repeated. The angular velocity of the sun varied with its declination angle; it was 67.3 μrad/sec on July 11 and 72.2 μrad/sec on September 5. We experienced difficulties in pointing accurately at the declination required to scan through the center of the solar disk, due to the lack of accurate setting circles and to boresight errors between the guide telescope and the main telescope.

Additional experiments were conducted around noon on December 2, 14, and 15, 1998. The angular velocity of the sun was was 67.3 μrad/sec on Dec 2 and 66.3 μrad/sec on the other two days. Our telescope was attached to a 30 inch telescope that was boresighted to a guide telescope and mounted in an observatory at the OTS. The boresight of our telescope was aligned to that of the 30 inch telescope by viewing stars. The aperture of the 30 inch telescope was covered during the perforated plate experiments and the guide telescope was fitted with a neutral density filter that permitted it to view the sun. This configuration allowed us to scan through the center of the sun with greater accuracy and stability than before. The sampling interval was reduced from 3 seconds to 2 seconds to improve the angular resolution. Otherwise, the procedure for the perforated plate measurements was the same as before.

On December 14 and 15, diffuser plate measurements were also made to estimate the effective albedo of the center of the solar disk when viewed through the perforated plate in each of the three spectral bands. In these observations, we removed the perforated plate assembly from the telescope, blocked its aperture, and nulled its dark current. We then observed sunlight scattered from a diffuser plate. The perforated plate was oriented vertically with its normal in the same vertical plane as the line of sight to the sun. In this geometry, the angle of incidence was simply the solar elevation angle, El_{sun}. Observation angles within a few degrees of specular reflection were avoided in the diffuser plate measurement.

The radiance from the diffuser plate was measured at each wavelength, both in direct sunlight, $L_{sun}(\lambda)$ and in the shadow of the observatory's dome, $L_{shade}(\lambda)$. $L_{shade}(\lambda)$ was typically about 5% of $L_{sun}(\lambda)$. The raw measurement in direct sunlight, $L_{sun}(\lambda)$, contained contributions due to illumination of the diffuser plate by both direct and indirect sunlight. The net measurement, $[L_{sun}(\lambda) - L_{shade}(\lambda)]$, removed the indirect sunlight component. The diffuse reflectivity of the diffuser plate, $p(\lambda)$, had previously been determined as a function of wavelength. Its value was 0.991 for the NIR (750 nm) and yellow/green (550 nm) bands and 0.988 for the blue (450 nm) band.[11] To estimate the radiance level, we assumed that the diffuser plate was an ideal Lambertian radiator, so that the observed radiance was independent of the angle of observation. The radiance corresponding to 100% albedo, $L_{alb}(\lambda)$, was then

determined for each spectral band from the equation:

$$L_{alb}(\lambda) = [L_{sun}(\lambda) - L_{shade}(\lambda)]/ [p(\lambda)\cos(El_{sun})] \quad (2)$$

More observations were made on September 23 and 24, 1999. The angular velocity of the sun was 72.7 μrad/sec. The experiment procedure was the same as before, except that a different geometry was used for the diffuser plate measurements. In these experiments, we mounted the diffuser plate at a distance of about 30 m from the telescope, with its normal vector close to the line of sight. The sun illuminated this plate at illumination angles, θ, greater than 45 degrees off-axis. In these observations, $L_{alb}(\lambda)$ was determined for each spectral band from the equation:

$$L_{alb}(\lambda) = L_{sun}(\lambda) / [p(\lambda)\cos(\theta)] \quad (3)$$

The NIR filter was mechanically unstable during these experiments, so valid measurements were only obtained in the two visible spectral bands.

6. EXPERIMENTAL DATA

We had difficulties in scanning through the center of the sun during the preliminary measurements performed in 1997 and on December 2, 1998. Therefore, we have not included that data in our analysis. These scan profiles had the same qualitative features as the subsequent measurements, however.

Figures 1, 2, and 3 are graphs of the solar radiance measurements taken on December 14, 1998. The effective albedo is plotted as a function of angle for two scans in each of the three spectral bands, centered at 450 nm, 550 nm, and 750 nm, respectively. The effective albedo was derived by averaging measurements of the net radiance from the diffuser plate measurements, using Eq.(2) and the procedure discussed above.

All of the scans through the solar disk had the same features. The angular structure of solar image was always smooth and symmetrical, with no observable interference pattern. The radiance level in the vicinity of the central maximum remained within 99% of its peak value over a "sweet spot" that subtended at least 600 μrad in the 450 nm band and larger angles in the other two bands. As anticipated, both the diameter of the FWHM and that of the sweet spot decreased with decreasing wavelength.

When multiple scans through the solar disk were made with the perforated plate filter, the signal level was very reproducible, as can be seen from the two scans per band in Figures 1-3. On December 15, 1998, we scanned the sun four times in each spectral band. Table 3 includes the standard deviations of the four measurements per band of the FWHM, the sweet spot diameter, and the effective albedo, (Although we do not have enough data to yield reliable statistics, the excellent scan-to-scan reproducibility of the measurements is very encouraging.) The observed signal levels in the diffuser plate measurements exhibited much greater variability. There was, of course, a seasonal variation in the absolute signal levels of both the perforated plate measurement and the diffuser plate measurement, due to the lower solar elevation angle in the winter months.

On September 23 and 24, 1999, we made measurements in the 450 nm and 550 nm channels, with the same procedure as before for the perforated plate measurement, but with the diffuser plate mounted at a distance. Since only three scans per band were made in this two-day interval, the results are averaged in the tabulation of the data. The diffuser plate measurements geometry was different, with the plate mounted at a distance from the telescope, as described in the preceding section, and Eq. 3 was used to compute the effective albedo.

Table 3. Summary of experimental results

Spectral band (nm)	Observation date	FWHM (mrad)	>99% (mrad)	Effective albedo
450	12/14/98	6.31	0.68	11.4
	12/15/98	6.37+/-0.06	0.71+/- 0.18	11.5 +/- 0.1
	9/23/99 & 9/24/99	6.17	0.62	8.00
550	12/14/98	6.74	0.86	9.35
	12/15/98	6.72+/-0.07	0.75+/-0.07	9.65 +/- 0.12
	9/23/99 & 9/24/99	6.67	0.81	7.40
750	12/14/98	9.95	0.99	6.38

	12/15/98	9.88+/-0.05	0.99+/-0.03	6.39 +/- 0.05

The FWHM and the absolute radiance level in consecutive scans were highly reproducible. The diameter of the 99% intensity contour is intrinsically difficult to measure because the slope of the radiance distribution as a function of angle is very flat in this region, around its maximum.

The diffuser plate measurements that were used to determine the effective albedo were highly dependent upon geometry. By comparing the right columns of Tables 2 and 3, it may be seen that our theoretical estimate of the effective albedo was smaller that the values measured with the diffuser plate in the observatory dome but larger that the values measured with the diffuser plate at a distance.

We would recommend using a large integrating sphere in future experiments to determine the effective albedo of perforated plates. Of course, we would also recommend using a perforated plate with a lower throughput, so that its effective albedo would be in the vicinity of 1.0.

7. APPLICATION TO FUTURE EARTH-IMAGING INSTRUMENTS

Based upon our preliminary experiments, there is a region at least 0.6 mrad in diameter in the center of the solar image where the radiance in all three spectral bands is constant to within 1 %. To achieve the greatest accuracy in calibrating an instrument, it should view dark space or a closed aperture door to subtract dark current and should then be scanned through the solar disk multiple times with the perforated plate deployed. To scan this maximum through each detector element, the cross-scan offset between adjacent scan lines should not exceed 0.6 mrad. For example, in the AGSI study, the focal plane subtends 14 mrad in the cross-scan direction, so it requires at least 23 scans through the solar disk. This procedure will allow each pixel in the array to view a radiance level within 1% of the peak, in an area of the solar disk where the radiance is relatively uniform.

To achieve a 1% precision in this measurement, it is desirable to make the uncertainty due to the signal to noise ratio (SNR) an order of magnitude lower, no greater than 0.1%. In other words, enough measurements of the center of the solar image should be averaged to produce a SNR of at least 1000. At high signal levels, silicon detectors in the visible and NIR spectral bands are shot noise limited, i.e., their SNR's approach the square root of the number of photo-electrons collected from the scene. Assuming a typical electronic well capacity of 150,000 electrons for detectors in the visible and NIR spectral bands, the maximum SNR that can be achieved in a single pixel equals the square root of this number, or 387. The peak of the solar curve subtends at least 600 μrad, or 43 times the 14-μrad pixel dimension in the along-scan direction. The maximum SNR of the average of 43 consecutive measurements is $387(43)^{1/2}$ or 2538. The solar energy levels lie near the high end of the dynamic range of the detectors, so the SNR of the average of the 50 pixels detected in a single scan should exceed the goal of 1000 by a comfortable margin.

Each scan should also cover at least one degree in the along-scan direction. Bi-directional scans may be used to minimize the total solar calibration time. In this procedure, each detector element measures the intensity as a function of angle as it scans through the solar disk. It is exposed to a wide range of radiance levels and color temperatures. Thus, the shape of the solar image is determined in each spectral band, as well as the peak.

Any measured change in the shape of the solar disk could be indicative of a specific instability in the system. For example, if the diameters of the holes in the perforated plate gradually decreased due to a build-up of contaminants, it would produce not only a decrease in throughput, but would also increase the measured solar disk diameter in each spectral channel, with greater increases at longer wavelengths. A shift in the spectral band of the filter in front of one array, due to color center formation, contamination, or mechanical instability, would cause the shape of the solar image to change for that array alone, while the shape of the solar image in the other bands remained constant.

The perforated plate calibration technique appears to have greater stability than any competitive technique. It is particularly attractive as a method of calibrating earth-viewing instruments in geosynchronous orbit. The GOES Imager can view the sun through the perforated plate with relative ease when the sun lies within the FOR, during local midnight for a period of about two months centered about each equinox. During summer and winter, the solar image is not available for periods of about four months, unless the attitude of the spacecraft is disturbed. (On an operational weather mission, it will probably not permissible to slew the spacecraft to perform a dedicated solar calibration.) Auxiliary sources may be used during these intervals. The perforated plate calibration, augmented by other, more frequent calibration measurements, may be used to determine the long-term on-orbit stability of

instruments. In has the potential to achieve a precision of better than 1% between beginning and end of life, throughout the reflective solar spectrum, from the SWIR to the UV, which appears to be better than any alternative approach can achieve.

ACKNOWLEDGEMENTS

This work was performed as a part of the Advanced Geosychronous Studies Imager feasibility studies conducted by NASA/GSFC. The Swales effort was supported under contract NAS5-32650. Mr. Del Jenstrom, the Study Manager, Dr. Dennis Chesters, the Study Scientist, and Mr. Sanford Hinkal, the Systems Engineer and the Swales task monitor, provided advice and support for this effort. Ms. Carmel Conaty of GSFC assisted us in specifying and procuring the perforated plate. Dr. James Butler of GSFC lent us a diffuser plate and provided on-going advice on many issues related to calibration. The Goddard Astronomy Club permitted us to use their facility for preliminary measurements and Mr. Thomas Zagwodzki assisted us in using an observatory at GSFC's Optical Test Center.

REFERENCES

1. D. Jenstrom, D. Chesters, S. Hinkal, et al, *Advanced Geosynchronous Studies Imager,* NASA/GSFC, p. 2-3, Nov. 1999.

2. C. R. Nagaraja Rao," Calibration Requirements fir the Visible and Near-Infrared Seonsors on GOES, Attachment 1, *In-flight Visible and Near Infrared Calibration of Future GOES Imagers Workshop Report,* D. D. Norris, ed , JPL/California Institute of Technology, Pasadena, CA, 1999.

3. M. S. Maxwell and H. H. Kieffer, "Calibrating the GOES Imager visible channel using the moon as an irradiance source", *Proc SPIE*, **3439**, *Earth Observing Systems 111*, pp 136-144, 1998.

4. J. C. Bremer, J. G. Baucom, H. Vu, M. Weinreb, H. Pinkine, "Estimation of long-term throughput degradation of GOES 8 & 9 visible channels by statistical analysis of star measurements", *Proc SPIE*, **3439**, *Earth Observing Systems 111*, pp 145-154, 1998.

5. M. Weinreb, NOAA/NESDIS, private communication.

6. G. Haas, W. R. Hunter, "Laboratory Experiments to Study Surface Contamination and Degradation of Optical Coating and Materials in Simulated Space Environments," *Applied Optics,* **Vol. 9, No. 9,** pp 2101-2110, 1970.

7. J. B. Heaney, H, Herzig, and J. F. Ozantowski, "Auger Spectroscopic Examination of MgF_2-Coated Mirrors before and after UV Irradiation, " *Applied Optics,* **Vol. 16, No. 7,** pp 1886-1889, 1977.

8. C. J. Bruegge, A. E. Stiegman, R. A. Rainen, and A. W. Springsteen, "Use of Spectralon as a diffuse reflectance standard for in-flight calibration of earth-orbiting sensors", *Optical Engineering*, **Vol. 32, No. 4,** pp 805-814, 1993.

9. K. Pierce, "Limb Darkening", *Allen's Astrophysical Quantities,* A. Cox, ed., pp 355-357, Springer-Verlag, New York, 1999.

10. J. C. Bremer and G. Si, " Technique for visible calibration of future GOES sensors by solar viewing through a perforated screen," *Proc SPIE*, **2812**, *GOES 8 and Beyond*, pp 618-629, 1996.

11. J. Butler, NASA/GSFC, private communication

Fig 1. Solar radiance scan with perforated plate at 450 nm

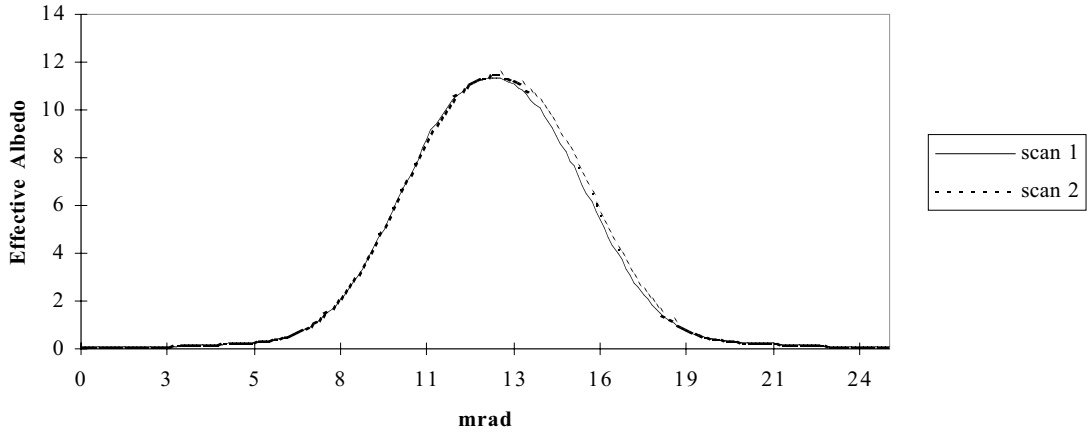

Fig 2. Solar radiance scan with perforated plate at 550 nm

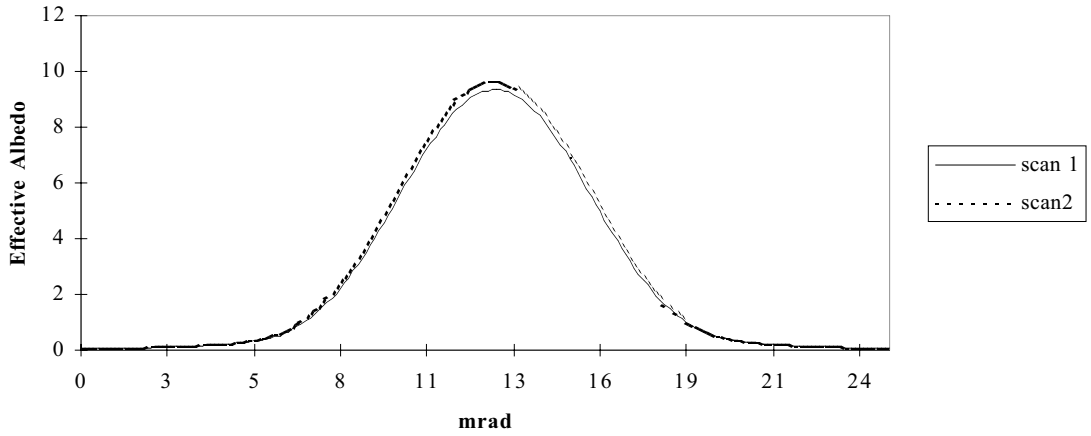

Fig. 3. Solar radiance scan with perforated plate at 750 nm